Time-resolved soft-x-ray spectroscopy of a magnetic octupole transition in nickel-like xenon, cesium, and barium ions

E. Träbert,* P. Beiersdorfer, and G. V. Brown
High Temperature and Plasma Physics Division, Lawrence Livermore National Laboratory, Livermore, California 94550-9234, USA

K. Boyce, R. L. Kelley, C. A. Kilbourne, F. S. Porter, and A. Szymkowiak
Goddard Space Flight Center, Greenbelt, Maryland 20771, USA
(Received 18 November 2005; published 15 February 2006)

A microcalorimeter with event mode capability for time-resolved soft-x-ray spectroscopy, and a high-resolution flat-field extreme ultraviolet spectrometer have been employed at the Livermore EBIT-I electron beam ion trap for observations and wavelength measurements of $M1$, $E2$, and $M3$ decays of long-lived levels in the Ni-like ions Xe^{26+}, Cs^{27+}, and Ba^{28+}. Of particular interest is the lowest excited level, $3d^9 4s\ ^3D_3$, which can only decay via a magnetic octupole ($M3$) transition. For this level in Xe, an excitation energy of (590.40±0.03 eV) and a level lifetime of (11.5±0.5 ms) have been determined.

DOI: 10.1103/PhysRevA.73.022508 PACS number(s): 32.30.Jc, 34.50.Fa, 34.80.Dp

I. INTRODUCTION

Usual atomic spectra are dominated by electric dipole ($E1$) transitions, connecting levels of opposite parity and involving a single electron that changes its angular momentum quantum number ℓ by one unit in the process. However, in a variety of cases, there are no $E1$ decay paths open to an excited atom or ion, and then higher-order terms of the multipole expansion of the radiation field are invoked to explain and describe transitions that may take place in spite of being forbidden by the $E1$ selection rules. The long-lived upper levels of such decays of low probability often serve as diagnostic tools in the study of terrestrial and astrophysical plasmas, because the level population may be density sensitive, if radiative transition and collision rates are of the same order of magnitude. Examples are the lowest triplet level in He-like ions [which can only decay by a magnetic dipole ($M1$) transition] and the spin-forbidden intercombination transition in He-like ions [1], as well as various $M1$ and $E2$ (electric quadrupole) transitions in many-electron ions [2]. Ions with extremely long-lived levels are among the contenders for atomic clocks, for example, in singly charged, trapped ions, such that decay only by an electric octupole ($E3$) transition [3,4]. In highly charged Ni-like ions, there is a level that decays only by a magnetic octupole ($M3$) transition. Such a decay has first been observed in the spectra of Ni-like ions of thorium ($Z=90$) and uranium ($Z=92$) [5]. We elected to study such a long-lived level in more detail.

In Ni-like ions, the ground configuration has a closed $3d^{10}$ shell, and the ground state has a term designation of $^1S_0$. The first excited configuration is $3d^9 4s$, with $^1D_2$ and $^3D_{1,2,3}$ levels (Fig. 1). For these levels to decay, the $4s$ electron (in a single-electron picture) would have to turn into a $3d$ electron, which involves a change of angular momentum quantum number ℓ by two units. Quantum mechanics gives these processes a low probability. For the $^3D_1$ level, the decay would change the total angular momentum J by one unit while preserving parity, and thus the appropriate multipole order of the radiation field would be the magnetic dipole, $M1$. For the $^1D_2$ and $^3D_2$ levels, the decay requires an electric quadrupole ($E2$) transition, whereas the $^3D_3$ level only decays by magnetic octupole ($M3$) radiation.

For low transition energies (in neutral atoms or ions of low charge), the transition probabilities of these high-multipole order transitions are very low. (For the $E3$ decay in Yb^+, the measured upper level lifetime is of the order of 7 years [3].) However, the rates increase with high powers of the ion charge q. Therefore, such transitions are no longer called "forbidden" in those very highly charged ions. In ions of moderate charge, however, the level lifetimes can be considerably longer than those of most other levels of the same ion, while being short enough to be measurable by practical

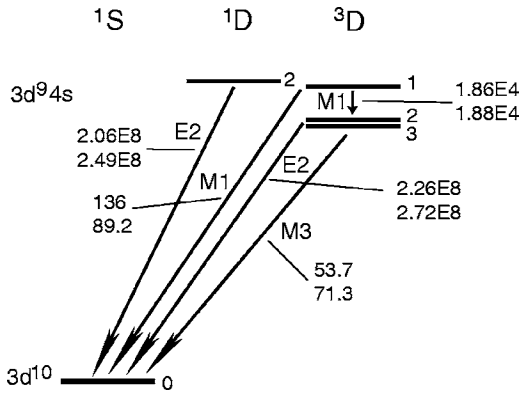

FIG. 1. Lowest levels and principal decays in Ni-like ions. The J values of the levels are noted at the right end of the level bars. The numbers associated with the principal decays are the calculated transition probabilities A_{ki} in the format aEb meaning $a\times 10^b$ s^{-1}. The first of each entry is from calculations by Safronova *et al.* [22,23], the second from our own GRASP code calulations (see text).

*Corresponding author. Electronic address: trabert1@llnl.gov

means [6–9]. In a given ion, levels that decay by $E1$ transitions may feature lifetimes in the picosecond range, while the levels that decay predominantly by $M1$ or $E2$ transitions may have lifetimes in the nanosecond or microsecond range. The $3d^9 4s\ ^3D_3$ level of the Ni-like ion Xe^{26+} ($Z=54$) (spectrum Xe XXVII) has a predicted lifetime of about 16 ms [10]. We have set out to check this prediction by a lifetime measurement. The transition energy of the $M3$ transition in Xe^{26+} has been predicted to be 587.5 eV, with a nearby $E2$ transition at 588.8 eV [10]. This places the lines of interest in the soft-x-ray range, for which we have set up a high-resolution spectrometer [11], recently.

Spectra of Ni-like ions have been studied before, employing various light sources from foil-excited ion beams [12], tokamaks [13], and laser-produced plasmas [14] to capillary discharges [15]. The beam-foil experiment by Cocke *et al.* included the observation of $3d$-$4s$ $E2$ transitions in Ni-like iodine. The laser-plasma experiment by Wyart *et al.* concerned Xe, but in the harder-x-ray range, not covering the lines of present interest. The tokamak experiment on Gd observed decays of short-lived levels, and the capillary-discharge measurement on Ag sought information in support of the $3d^9$ $4p$-$4d$ Ni-like ion laser experiments (for references, see [15]). In most of these experiments, the density would have been too high to see the $M3$ decay against the competition by collisional quenching, even if suitable spectroscopic equipment had been used.

The structure of Ni-like ions has been calculated by a number of different algorithms. Biémont and Quinet [16,17] treat Ni-like ions, but only a few and far apart ones, and not those of Xe among them, or not the $M3$ decays. Zhong *et al.* [18] treat Ni-like ions of Ta, but without the high multipole order transitions. Safronova *et al.* have repeatedly calculated transition in Ni-like ions. In earlier papers [19,20], the $3d^9 4s$ levels or the $M3$ decay were not treated, which is why we solicited specific calculations of the $M3$ transition energies [21]. The latest large-scale presentation of calculational results for Ni-like ions by Safronova *et al.* [22] includes the $M3$ transition rates. However, Fig. 1 reveals that the dominant decay branch of the $3d^9\ 4s\ ^3D_1$ level leads to the $^3D_2$ level, greatly affecting the relative line intensities of the soft-x-ray transitions; however, these in-shell transition rates are not included in that latest publication. We have again solicited calculations, now on the "missing" $M1$ in-shell transition rates [23], and we have performed our own calculations using the GRASP code (in the -AL average level option) [24,25], so that we can present reasonably complete theoretical values along with our experimental results.

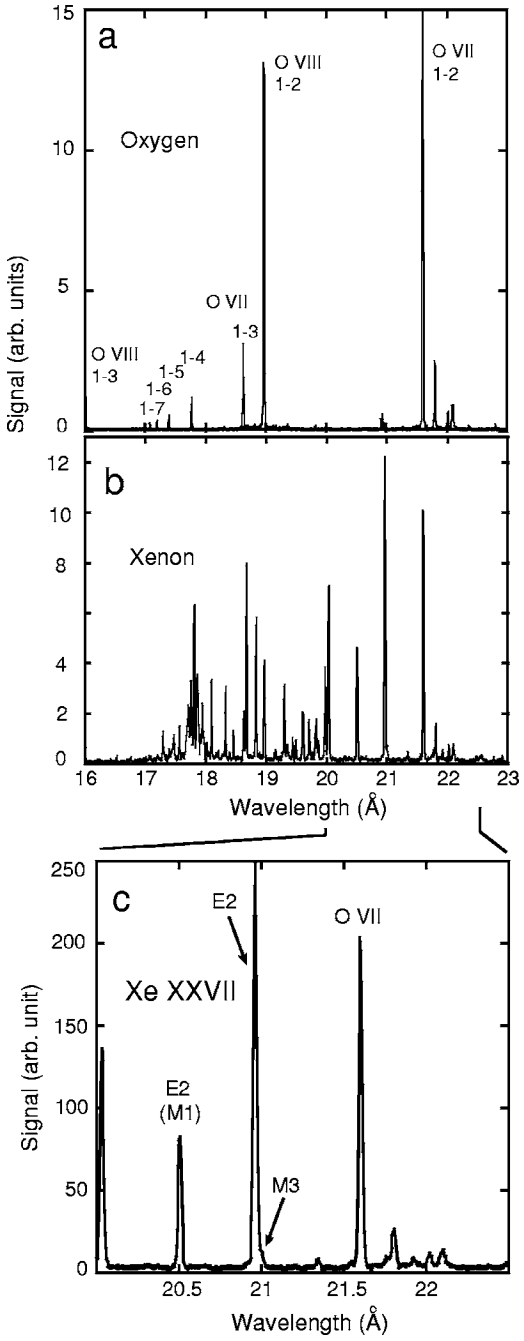

FIG. 2. Soft-x-ray spectra recorded with the flat-field spectrometer. (a) CO_2 injection results in O VII and O VIII lines in the spectrum; (b) Xe injection; some of the strongest oxygen lines persist. The strongest line in the spectrum is from the $E2$ decay in Xe^{26+}. It has a partly resolved companion line of about 5% of the intensity of the $E2$ line; we identify this companion line with the $M3$ transition of interest. Panel (c) shows the region of present interest in more detail.

II. EXPERIMENT

The experiment was done at the University of California Lawrence Livermore National Laboratory low-energy electron beam ion trap [26]. Most of the present work was performed at electron beam energies up to 1450 eV, that is, below the ionization potential of Xe^{26+} at 1499 eV [10], and at electron beam currents from 0.6 mA up to about 40 mA. For the atomic lifetime measurements, we employed the "magnetic trapping" mode [27], in which after a period of ion production and excitation by means of the electron beam, the latter is switched off, and the ions are then kept trapped by the drift tube potentials and the 3 T magnetic field, as they are in a Penning trap. The trap cycle time included about 40 to 50 ms for the breeding of ions in the desired charge state (*electron beam on*), 50 to 70 ms for the obser-

TABLE I. Predicted and measured values for the excitation energies of the $3d^9 4s$ levels in Xe^{26+}. Our own theory values have been obtained using the GRASP code [24].

Level Number	LS Term Designation	Theory Energy (eV)[a]	Energy (eV)[b]	Energy (eV)[c]	Experiment Energy (eV)[a]
5	$3d^9 4s\ ^1D_2$	603.560		604.271	604.59±0.03
4	$3d^9 4s\ ^3D_1$	602.706		603.359	blended
3	$3d^9 4s\ ^3D_2$	589.986	588.8	591.020	591.44±0.03
2	$3d^9 4s\ ^3D_3$	588.890	587.5	589.98	590.40±0.03
1	$3d^{10}\ ^1S_0$	0	0	0	

[a]This work.
[b]Reference [10].
[c]Reference [22].

vation of delayed emission (*electron beam off*), plus time for dumping the ion cloud from the trap before creating a new population of ions.

Xe gas was continually injected into the trap volume from a reservoir at a pressure of up to 1.8×10^{-7} Torr. Based on previous experience, this makes for a gas pressure in the center of the injected gas plume that is of the order of 10^{-9} Torr, compared to an ambient pressure in the ion trap that is about two orders of magnitude lower [28]. The process of always breeding from neutral atoms provides for a charge state distribution that comprises all charge states up to the maximum. Following the time development of the x-ray spectrum by means of the XRS microcalorimeter (see below), we made certain that the maximum charge state was, in fact, reached within a fraction of the breeding period under the given experimental conditions.

The experiment proceeded in two parts: (a) recording of high-resolution extreme ultraviolet (EUV) spectra and determination of line positions and wavelengths, and (b) measurement of the $^3D_3$ level lifetime by time-resolved observations at lower spectral resolution using a higher detection efficiency microcalorimeter.

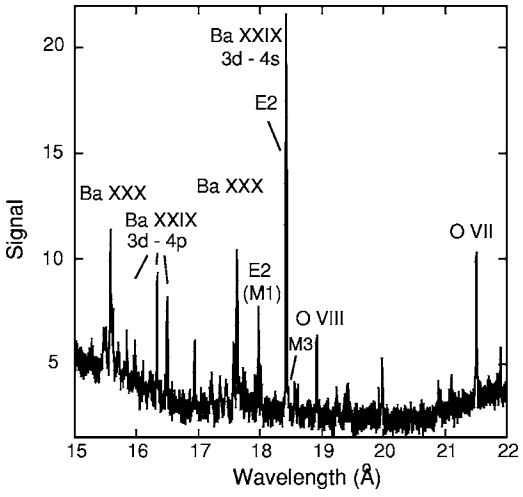

FIG. 3. EUV spectrum of Ba obtained with the same flat-field spectrometer as used for Fig. 2 at an electron beam energy of 1500 eV. The wavelength scale is only approximate.

Grating spectrometer observations

For the high-resolution EUV spectroscopy part of the experiment, a flat-field grazing incidence spectrometer was used that was equipped with a gold-coated variable line spacing grating [29] of $R=44.3$ m radius of curvature and 2400 lines/mm average groove density, set up at an angle of incidence of about 88° [11]. Earlier versions of such spectrometers that were used at this electron beam ion trap had gratings with $R=5$ m or $R=15$ m [30,31]; in comparison to these, the present instrument has a resolving power that is about a factor of 6–8 higher.

This spectrometer is equipped with a detector that comprises a cryogenically cooled, thinned, back-illuminated charge-coupled device (CCD) of 1340×1300 pixels on a 25 mm×25 mm substrate. The wavelength coverage varies with the mean wavelength setting; it is about 7 Å in our range of interest. Each pixel then corresponds to a wavelength interval of about 5.4 mÅ. As we image the electron beam with about unity magnification onto the detector, the

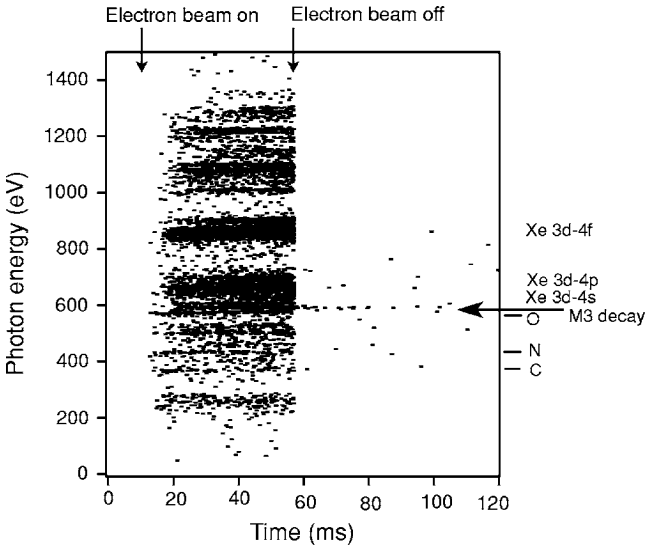

FIG. 4. Scatter plot of x-ray photon energy measured with the XRS microcalorimeter versus time in the electron beam ion trap cycle. At $t=55$ ms, the electron beam is switched off and, therefore, direct excitation ends.

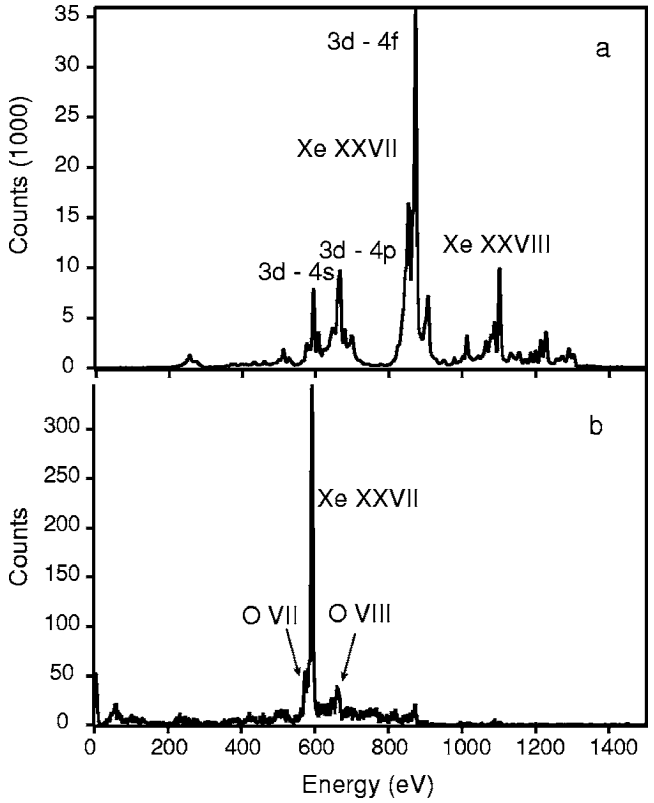

FIG. 5. Time-resolved soft-x-ray data obtained with the XRS microcalorimeter at an electron beam energy of 1450 eV. (a) Electron beam on (corresponding to time interval 30 to 50 ms in Fig. 4); (b) electron beam off (t=57–120 ms). The line of interest is the strongest line in the bottom spectrum. The actual data are from much longer accumulation times than the data in Fig. 4 and also from a somewhat slower timing cycle.

typical linewidth is about 5 pixels, or 27 mÅ, and the resolving power is about 800 for wavelengths near 20 Å. For long-lived emitters, the emission zone is wider than the electron beam because of ion motion; this shows in the somewhat wider spectral line images, too [32]. Typical exposure times were 20 to 30 min.

The Xe lines of interest are close to the resonance lines of He-like O VII and H-like O VIII. Reference spectra were recorded while CO_2 was injected into the electron beam ion trap, providing the O VII $1s^2$-$1snp$ line series (n=2 to n=8) [33–35] and the O VIII $1s$-$2p$ (Ly-α) line [36] in the same spectrometer setting as used with Xe injection. In fact, the strongest oxygen lines remained visible from the residual gas even when nominally running Xe, providing calibration lines in the very Xe spectra of interest. Sample spectra of O and Xe as recorded with the flat-field spectrometer are shown in Fig. 2. The wavelength measurement results (converted to an eV scale) are included in Table I.

The line of primary interest shows as a small partner [about 5% in Fig. 2(c)] of a line blend with the $E2$ transition from the $3d^9 4s\ ^3D_2$ level. The line intensity ratio varies with the electron beam current; it is highest at low currents (about 20% at 1 mA), and lowest at high electron beam currents (about 1% at 40 mA). The relative line intensities thus reflect

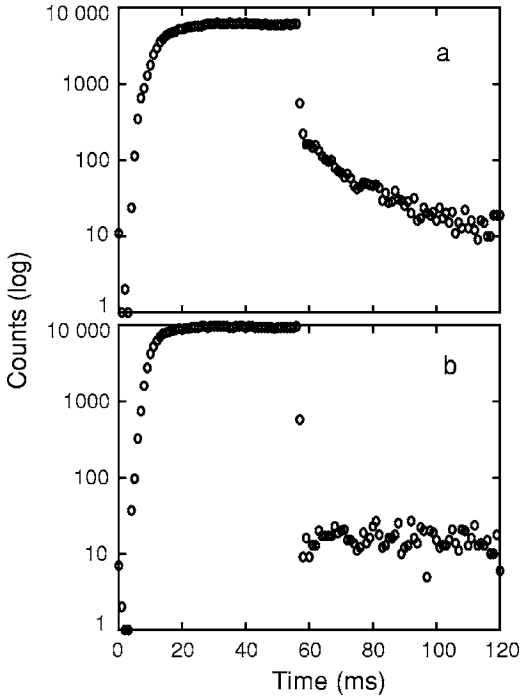

FIG. 6. Time-resolved soft-x-ray data obtained with the XRS microcalorimeter at an electron beam energy of 1450 eV. Decay curves obtained by using photon-energy cuts of data like those in Fig. 4. (a) 585–595 eV (which includes the Xe $M3$ line at 590 eV), (b) 650–660 eV (which includes the Ly-α transition of OVIII).

the fact that the $^3D_3$ level is not only excited by the electron beam, but is so long lived that it can also be notably depopulated by electron-ion collisions. In contrast, the $^3D_2$ level with its predicted radiative lifetime in the nanosecond range decays predominantly by emission of radiation. The population of the $^3D_2$ level is further increased by a sizeable cascade contribution from the $^3D_1$ level in the same configuration; the other three $3d^9 4s$ levels decay predominantly to the ground state. The measured line separation corresponds to a

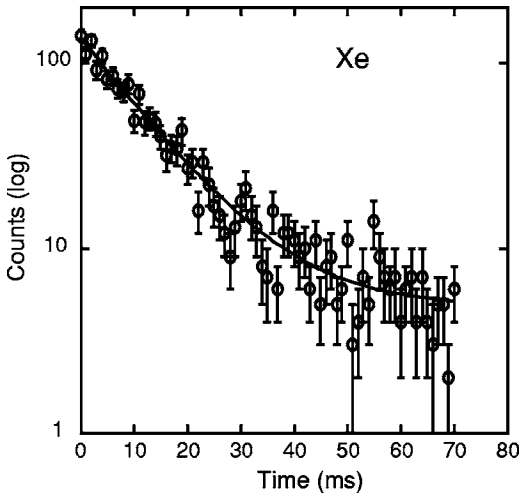

FIG. 7. Decay of the $M3$ line [from Fig. 6(a)]. The solid line represents a single exponential (plus background) fitted to the data.

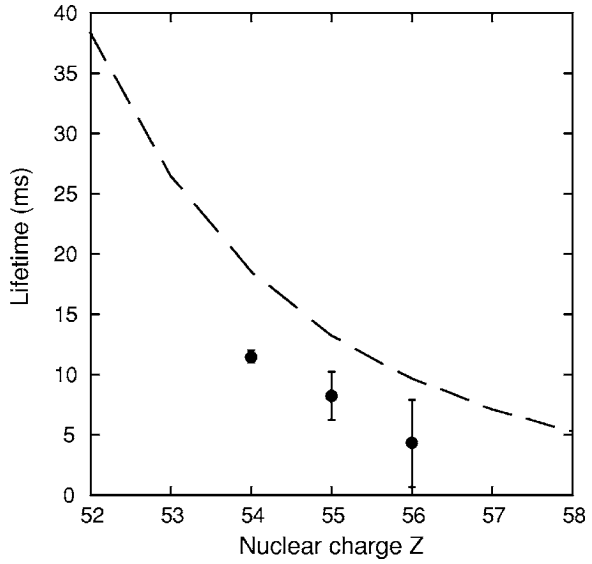

FIG. 8. Lifetime of the $3d^9 4s\ ^3D_3$ level as predicted by Safronova *et al.* [22,23] (dashed line) in comparison with our measurements for Xe, Cs, and Ba.

fine structure interval of 1.04 eV, which roughly corroborates the predictions. The next neighbor line at 604.59 eV arises from the decays of the $3d^9 4s\ ^3D_1$ and $^1D_2$ levels (Figs. 1 and 2). Our calculation predicts the $^1D_2$ level to lie higher than the $^3D_1$ level by some 0.9 eV, whereas an interpolation of the calculations by Biémont [16] suggests the inverse sequence. We see no line broadening nor a second line, which is no surprise, given the 99% branch fraction that favors the in-shell $M1$ decay (far out of our observation range) of the $^3D_1$ level to the $^3D_2$ level. The strongest Xe line in our spectra, therefore, represents the population of, both, $^3D_2$ and $^3D_1$, levels. The actual $^3D_1$ and $^1D_2$ level sequence remains uncertain at present.

In addition to the Xe measurements, we recorded data on Ni-like ions of barium. Barium, with an ionization potential of the Ni-like ion of 1.70 keV [10], evaporates from the electron gun cathode and is a regular contaminant of electron beam ion traps. The Ba spectra corroborate our xenon findings. A sample flat-field spectrometer spectrum of Ba is shown in Fig. 3.

III. MICROCALORIMETER OBSERVATIONS

For broadband x-ray observations and for time-resolved spectra, we used an x-ray spectrometer microcalorimeter built by NASA/Goddard Space Flight Center and known as the XRS/EBIT [37,38]. The XRS/EBIT represents an upgraded version of an earlier instrument which had about half the resolving power (10 eV then, nominally 6 eV now). For the measurements presented here, 13 individually energy-calibrated pixels were available and operated at a temperature of 0.059 K, each with a detection range for photons of a few hundred electron volts up to about 12 keV. The remaining pixels (of a total of 36) were not used for the present experiments, either because they used different absorbers (Bi instead of HgTe), or were not connected with the read-out electronics. Each detected signal event is time stamped and thus available for off-line data evaluation in the correct phase relation to the electron beam ion trap cycles. Because of the low count rate of our measurement, care was taken to reduce cosmic rate events that would increase the background level.

Figure 4 shows a scatter plot of the x-ray pulses measured with the microcalorimeter as a function of time during an electron beam ion trap cycle, which comprises dumping of the old trap content (at $t=0$), admitting the electron beam at about $t=12$ ms, breeding of ions with the electron beam on

TABLE II. Predicted and measured values for the upper level lifetimes of the $3d^9 4s$ levels in Xe^{26+}, Cs^{27+}, and Ba^{28+}. Our own theory values (unmarked) have been obtained using the GRASP code [24,25].

Level Number	LS Term Designation	Theory Lifetime[a]	Lifetime[b]	Lifetime[c]	Strongest Decay Branch to Level	Experiment Lifetime[a]
Xe^{26+}						
5	$3d^9 4s\ ^1D_2$	4.02 ns		4.85 ns	1	
4	$3d^9 4s\ ^3D_1$	52.9 μs		53.4 μs	3	
3	$3d^9 4s\ ^3D_2$	3.68 ns		4.42 ns	1	
2	$3d^9 4s\ ^3D_3$	14.0 ms	16.4 ms	18.6 ms	1	11.5±0.5 ms
1	$3d^{10}\ ^1S_0$					
Cs^{27+}						
2	$3d^9 4s\ ^3D_3$			13.3 ms	1	8.2±2.0 ms
Ba^{28+}						
2	$3d^9 4s\ ^3D_3$			9.6 ms	1	4.3±3.6 ms

[a]This work.
[b]Reference [10].
[c]Reference [22,23].

(until $t=55$ ms), and observation of delayed photon emission after the electron beam is switched off. The figure actually represents only a short accumulation time; the total of our observations amounts to millions of signal pulses. In most of our observations, the breeding lasted till $t=65$ ms, and the observation of delayed emission continued until $t=141$ ms. As long as the electron beam is running, the XRS spectrum reflects the buildup of the charge state distribution and shows lines from many charge states. When the electron beam is switched off, ionization and excitation cease, and so do practically all emissions. A very low background arises from charge exchange of the highly charged ions of the trapped ion cloud with the atoms of the residual gas. At one photon energy, however, slightly higher than the x-ray energy of the O VII "w" line, a weak tail shows in the scatter plots. This tail persists for a few dozen milliseconds before fading out; this tail is the signature of the $M3$ decay of interest in Xe^{26+}. Figure 5 represents this situation by spectral cuts through the scatter plot. The $M3$ line forms the dominant line in the "electron beam off" part of Fig. 5.

In the first of two measurement campaigns, the XRS spectra yielded a linewidth [full width at half maximum (FWHM)] of 12 eV, because a low gain was used to access high-energy x-rays unrelated to the present experiment. Preliminary results were reported in Ref. [21]. In a second campaign, dedicated to this measurement, the XRS was optimized and the linewidth was 7 ± 1 eV, after summing several days worth of data from all 13 active channels. No drift correction of the pulse height gain was conducted.

Photons from the $M3$ transition are not the only ones detected after the end of direct excitation. Figure 6 shows light curves at the photon energies of the O VIII Ly-α-transition (656 eV) and of the $M3$ transition (590 eV) in Xe XXVII, each collected from a 10 eV wide band (of first-campaign data) that included the energy of interest. The decay curve for the oxygen transition is very steep at the end of the electron beam excitation, because the upper level radiative lifetime is in the picosecond time range. Then a practically flat tail follows that represents level population and radiative decay after charge exchange (CX), that is, after collisions of bare oxygen ions with neutral atoms of the residual gas have produced O VIII in levels that then can emit X radiation. CX involving oxygen ions has been studied in our device before [39]. At our vacuum conditions, the time constant of CX corresponds to an ion lifetime in the range of seconds. In contrast, the decay curve of the $M3$ line in Xe shows a visually recognizable exponential behavior, clearly indicating a long upper level radiative lifetime in the millisecond range.

Figure 7 shows the decay part of the $M3$ light curve. Here the data of the second campaign were used, which had a better signal-to-background ratio than the other. Again, a 10 eV energy band was used, although this interval is wider than the FWHM linewidth. However, the spectrum shows no blends within this interval, so that more signal counts (at the cost of including more of the low background) could be accumulated.

The data sets have been analyzed by multiexponential curve fitting techniques. However, not more than one exponential (plus a constant background) was found to be appropriate on statistical grounds. This also matches the physical situation as the following discussion shows. (1) There are no (known) long-lived higher lying excited levels of Xe^{26+} that would give rise to cascade repopulation. (2) CX and other ion loss mechanisms have a much longer time scale than encountered in our decay curves, as the oxygen emission produced by CX [Fig. 6(b)] has shown. (3) Repopulation of the Xe^{26+} metastable level by recombination of Xe^{27+} is possible, but also proceeds on a time scale that is much longer than encountered here for the same reasons as given in (2). For recombination to be important in first place, there would have to be higher charge states to act as recombination targets. The electron beam energy is below the ionization potential of Xe^{26+}. However, Xe^{27+} is being produced in a multistep process, with the very metastable state of principal interest as a stepping stone. If anything, recombination in part counterbalances loss due to (2). (4) If after recombination, the electron reaches the $3d^9 4f$ levels, the decay proceeds to the $3d^{10}$ ground state directly, not to the $3d^9 4s$ level. $3d^9 4d$ electrons decay toward the $3d^9 4p$ levels, but these then decay preferentially to the ground state, with only very minor decay branches feeding the $4s$ levels. We consequently base our analysis and result on fits using a single exponential.

The numerous data sets of the lower resolution campaign were combined into four large sets. One of these sets comprises data that were measured with a filter that screened against low-energy photons and reduced the $M3$ line somewhat. The other three sets were measured without such a filter in place. These four data sets were analyzed separately in order to learn about systematic errors and the reproducibility of the fit results. No significant differences were found. Therefore, all data sets of the higher-resolution campaign were added up front and evaluated as one. The fit results differ by slightly more than the combined (statistical) error bars. However, systematic errors are smaller for the second measurement, and our weighted final lifetime result is dominated by the results from the second campaign. We find a Xe $^3D_3$ level lifetime of 11.5 ± 0.5 ms, which corrresponds to a rate of 81 ± 4 s^{-1} for the magnetic octupole decay from this level.

The XRS was also used for time-resolved measurements on cesium, Cs^{27+}. However, the measurements were less extensive than those for xenon. Because the Cs experiment was conducted immediately after the Xe measurements, some Xe was still present as a contaminant in the trap. However, the energy discrimination provided by the XRS permitted us to extract decay curve data from an energy interval around the 630 eV expected for the $M3$ decay in Cs^{27+}. This yielded a $Cs^{27+} 3d^9 4\ ^3D_3$ level lifetime of 8.2 ± 2 ms. Finally, the residual fraction of Ba in the trap contributed sufficient signal near 670 eV to derive a lifetime of the corresponding Ba level of 4.3 ± 3.6 ms. An overview of the measured lifetimes is given in Fig. 8.

IV. SUMMARY OF RESULTS

A summary of the results is given in Tables I and II. The transitions of interest take place between shells ($\Delta n=1$), and

theory can estimate such transition energies rather well. The differences range between 1 and 2 eV, as the comparison of the calculated and measured transition energies in Table I shows. By contrast, the measured $M3$ transition rate differs significantly from the calculated values, as seen in Table II. The $Xe^{26+}3d^9 4s\ ^3D_3$ level lifetime of 11.5 ± 0.5 ms is, for example, shorter than predicted by Safronova *et al.* [22,23] by a third, whereas a simple GRASP code [24] calculation of ours produces the closest result. The Cs^{27+} and $Ba^{28+}3d^9 4s\ ^3D_3$ level lifetimes corroborate the same trend (Fig. 8).

The fact that the level lifetime is shorter than predicted means that the level is less susceptible to de-excitation by collisional effects. As a result, there is a shift to higher-electron densities where the $M3$ line could be employed as an electron density diagnostic. Interestingly, the role of the $^3D_3$ metastable level in collisional excitation and ionization has altogether been neglected so far, even in recent calculations of such processes [40].

ACKNOWLEDGMENTS

We are happy to acknowledge the dedicated technical support by Ed Magee, Merv Lawrence, and Phil D'Antonio. S. Terracol (LLNL) and C. L. Harris (Reno) helped with running some of the measurements. E. T. acknowledges travel support by the German Research Foundation (DFG). The work at the University of California Lawrence Livermore National Laboratory was performed under the auspices of the Department of Energy under Contract No. W-7405-Eng-48.

[1] J. U. Ness, R. Mewe, J. H. M. M. Schmitt, A. J. J. Raassen, D. Porquet, J. S. Kaastra, R. L. J. van der Meer, V. Burwitz, and P. Predehl, Astron. Astrophys. **367**, 282 (2001).
[2] M. Klapisch, J. L. Schwob, M. Finkenthal, B. S. Fraenkel, S. Egert, A. Bar-Shalom, C. Breton, C. DeMichelis, and M. Mattioli, Phys. Rev. Lett. **41**, 403 (1978).
[3] M. Roberts, P. Taylor, G. P. Barwood, W. R. C. Rowley, and P. Gill, Phys. Rev. A **62**, 020501(R) (2000).
[4] M. Roberts, P. Taylor, G. P. Barwood, P. Gill, H. A. Klein, and W. R. C. Rowley, Phys. Rev. Lett. **78**, 1876 (1997).
[5] P. Beiersdorfer, A. L. Osterheld, J. Scofield, B. Wargelin, and R. E. Marrs, Phys. Rev. Lett. **67**, 2272 (1991).
[6] E. Träbert, in *Accelerator-based Atomic Physics Techniques and Applications*, edited by S. M. Shafroth and J. C. Austin (American Institute of Physics, Washington, DC, 1997), pp. 567.
[7] E. Träbert, Phys. Scr. **61**, 257 (2000).
[8] E. Träbert, Phys. Scr., T **100**, 88 (2002).
[9] E. Träbert, Can. J. Phys. **80**, 1481 (2002).
[10] J. H. Scofield (private communication).
[11] P. Beiersdorfer, E. W. Magee, E. Träbert, H. Chen, J. K. Lepson, M. F. Gu, and M. Schmidt, Rev. Sci. Instrum. **75**, 3723 (2004).
[12] C. L. Cocke, S. L. Varghese, J. A. Bednar, C. P. Bhalla, B. Curnutte, R. Kauffman, R. Randall, P. Richard, C. Woods, and J. H. Scofield, Phys. Rev. A **12**, 2413 (1975).
[13] S. von Goeler, P. Beiersdorfer, M. Bitter, R. Bell, K. Hill, P. LaSalle, L. Ratzan, J. Stevens, J. Timberlake, S. Maxon, and J. Scofield, J. Phys. Chem. Ref. Data **40**, C1–181 (1988), supplement.
[14] J. F. Wyart, C. Bauche-Arnoult, J. C. Gauthier, J. P. Geindre, P. Monier, M. Klapisch, A. Bar-Shalom, and A. Cohn, Phys. Rev. A **34**, R701 (1986).
[15] A. Rahman, J. J. Rocca, and J. F. Wyart, Phys. Scr. **70**, 21 (2004).
[16] E. Biémont, J. Phys. B **30**, 4207 (1997).
[17] P. Quinet and E. Biémont, Phys. Scr. **43**, 150 (1991).
[18] J. Y. Zhong, J. Zhang, J. L. Zeng, G. Zhao, and M. F. Gu, At. Data Nucl. Data Tables **89**, 101 (2005).
[19] U. I. Safronova, W. R. Johnson, and J. R. Albritton, Phys. Rev. A **62**, 052505 (2000).
[20] S. M. Hamasha, A. S. Shlyaptseva, and U. I. Safronova, Can. J. Phys. **82**, 331 (2004).
[21] E. Träbert, P. Beiersdorfer, G. V. Brown, S. Terracol, and U. I. Safronova, Nucl. Instrum. Methods Phys. Res. B **235**, 23 (2005).
[22] U. I. Safronova, A. S. Safronova, S. M. Hamasha, and P. Beiersdorfer, At. Data Nucl. Data Tables **92**, 47 (2006).
[23] U. I. Safronova (private communication).
[24] I. P. Grant, in *Methods in Computational Chemistry*, edited by S. Wilson (Plenum Press, New York, 1988), Vol. 2 p. 1.
[25] F. Parpia, C. Froese Fischer, and I. P. Grant, Comput. Phys. Commun. **94**, 249 (1996).
[26] M. A. Levine, R. E. Marrs, J. N. Bardsley, P. Beiersdorfer, C. L. Bennett, M. H. Chen, T. Cowan, D. Dietrich, J. R. Henderson, D. A. Knapp, A. Osterheld, B. M. Penetrante, M. B. Schneider, and J. H. Scofield, Nucl. Instrum. Methods Phys. Res. B **43**, 431 (1989).
[27] P. Beiersdorfer, L. Schweikhard, J. Crespo López-Urrutia, and K. Widmann, Rev. Sci. Instrum. **67**, 3818 (1996).
[28] E. Träbert, P. Beiersdorfer, G. Gwinner, E. H. Pinnington, and A. Wolf, Phys. Rev. A **66**, 052507 (2002).
[29] T. Harada and T. Kita, Appl. Opt. **19**, 3987 (1980).
[30] P. Beiersdorfer, J. R. Crespo López-Urrutia, P. Springer, S. B. Utter, and K. L. Wong, Rev. Sci. Instrum. **70**, 276 (1999).
[31] S. B. Utter, P. Beiersdorfer, G. V. Brown, E. J. Clothiaux, and N. K. Podder, Rev. Sci. Instrum. **70**, 284 (1999).
[32] J. R. Crespo López-Urrutia, P. Beiersdorfer, K. Widmann, and V. Decaux, Can. J. Phys. **80**, 1687 (2002).
[33] G. W. F. Drake, Can. J. Phys. **66**, 586 (1988).
[34] L. Engström and U. Litzén, J. Phys. B **28**, 2565 (1995).
[35] R. L. Kelly, online database at http://cfa-www.harvard.edu/amdata/ampdata/kelly/kelly.html
[36] J. D. Garcia and J. E. Mack, J. Opt. Soc. Am. **55**, 654 (1965).
[37] F. S. Porter, M. D. Audley, P. Beiersdorfer, K. R. Boyce, R. P. Brekosky, G. V. Brown, K. C. Gendreau, J. Gygax, S. Kahn, R. L. Kelley, C. K. Stahle, and A. E. Szymkowiak, Proc. SPIE **4140**, 407 (2000).
[38] F. S. Porter, G. V. Brown, K. R. Boyce, R. L. Kelley, C. A. Kilbourne, P. Beiersdorfer, H. Chen, S. Terracol, S. M. Kahn,

and A. E. Szymkowiak, Rev. Sci. Instrum. **75**, 3772 (2004).
[39] P. Beiersdorfer, K. R. Boyce, G. V. Brown, H. Chen, S. M. Kahn, R. L. Kelley, M. May, R. E. Olson, F. S. Porter, C. K. Stahle, and W. A. Tillotson, Science **300**, 1558 (2003).
[40] N. R. Badnell, K. A. Berrington, H. P. Summers, M. G. O'Mullane, A. D. Whiteford, and C. P. Ballance, J. Phys. B **37**, 4589 (2004).